

Received:
5 December 2017
Revised:
19 July 2018
Accepted:
28 November 2018

Cite as: Dong Chen,
Yu-Jia Wang, Yin-Lian Zhu,
Xiu-Liang Ma. Effect of
transition metal (TM) doping
on structural and magnetic
properties in hexagonal
 $\text{YMn}_{0.917}\text{TM}_{0.083}\text{O}_3$ systems.
Heliyon 4 (2018) e00993.
doi: [10.1016/j.heliyon.2018.e00993](https://doi.org/10.1016/j.heliyon.2018.e00993)



Effect of transition metal (TM) doping on structural and magnetic properties in hexagonal $\text{YMn}_{0.917}\text{TM}_{0.083}\text{O}_3$ systems

Dong Chen*, Yu-Jia Wang, Yin-Lian Zhu, Xiu-Liang Ma**

Shenyang National Laboratory for Materials Science, Institute of Metal Research, Chinese Academy of Sciences,
Wenhua Road 72, 110016 Shenyang, China

* Corresponding author.

** Corresponding author.

E-mail addresses: dchen@imr.ac.cn (D. Chen), xlma@imr.ac.cn (X.-L. Ma).

Abstract

Suitable TM doping at the Mn site is an important access to manipulate magnetic properties of hexagonal YMnO_3 , however, it has not yet been systematically explored how the strength of antiferromagnetic interactions and the magnetic transition temperatures (T_N) are modified in the doping $\text{YMn}_{0.917}\text{TM}_{0.083}\text{O}_3$ systems. In the work, we have performed first-principles calculations to study the effect of TM doping on the structural and magnetic properties of hexagonal $\text{YMn}_{0.917}\text{TM}_{0.083}\text{O}_3$ bulks; the results are combined with the available experimental results. The calculated results reveal that the planar TM-O bonds and O-TM-O angles of TMO_5 bipyramid are both prominent structural features for the transformations of magnetic properties. We have also predicted the Ti, V, Cr and Fe doping effects on magnetic properties and further analyzed the TM electronic structures of TMO_5 bipyramid in the $\text{YMn}_{0.917}\text{TM}_{0.083}\text{O}_3(001)/\text{MgO}(001)$ film configurations, which could provide more understanding towards the designing of new generation multifunctional devices.

Keyword: Condensed matter physics

1. Introduction

Multiferroic materials exhibit simultaneous ferroic responses with coupled electric, magnetic, and structural orders. They are very important because of their unique and strong coupling of electric and magnetic properties, giving rise to the simultaneous presence of more than one ferroic property. Hexagonal YMnO₃ is the most extensively studied multiferroic material among all hexagonal manganites [1], which possesses magnetism and ferroelectricity simultaneously with a high ferroelectric transition temperature (~ 900 K) and a low antiferromagnetic (AFM) transition temperature (~ 70 K). The crystal structure of YMnO₃ ($P6_3cm$) can be described as stacks of corner-linked MnO₅ trigonal bipyramid (Mn atoms with two apical oxygen (O1 and O2) atoms and three planar oxygen (O3 and O4) atoms) layers separated by Y atom layers along the crystallographic c -axis. In the hexagonal structure there appears to be a small tilting (a cooperative tilting distortion which buckles the trigonal planes) of MnO₅ bipyramids, which consist of five Mn–O bonds: Mn–O1 and Mn–O2 oriented along the c direction while Mn–O3 and two pairs of Mn–O4 bonds lie within the ab plane. The noncollinear magnetic order is originating from the strong antiferromagnetic superexchange interaction of Mn spins in the ab plane of YMnO₃ structure below the Néel temperature T_N of 70 K [2, 3]. As the symmetry breaking distortion is driven by geometric but not electronic factors in hexagonal YMnO₃, there is some freedom to tune the magnetic behavior of manganese atoms by electronic doping, without losing the acentric structure of host phase [4]. Doping atoms with different atomic radius will inevitably change the lattice constant and also the Mn–Mn bond distance. This change in the Mn–Mn bond distance, in particular on the ab plane, leads naturally to variations in the exchange integral, which is a critical parameter for the formation of magnetic ground state [5]. Therefore doping at the Mn site in the hexagonal YMnO₃, one can manipulate the physical properties and change the magnetic ground state.

In recent years, a few studies have been reported on the influence of transition metal (TM) elements doping at Mn-site in hexagonal manganite bulks [5, 6, 7, 8, 9, 10, 11, 12, 13], in which most of doping concentrations were kept about 10% to preserve the phase isostructural. For examples, N. Sharma *et al.* [6] pointed out that doping with 10% Ti at Mn site could reduce the temperature T_N from 75 K of YMnO₃ compound to 55 K of polycrystalline YMn_{0.9}Ti_{0.1}O₃ synthesized through a solid state reaction. T. C. Han *et al.* [7] found that the antiferromagnetic transition temperature of YMn_{1-x}Cr_xO₃ ($0 \leq x \leq 0.1$) increased from 73 K to 89 K with increasing Cr-content (x). And F. Wan *et al.* [8] also reported that the T_N of YMn_{1-x}Cr_xO₃ ($x = 0-0.1$) compounds would increase from 73.1 K to 86.1 K. S. Namdeo *et al.* [9] put forward that the Néel temperatures of YMn_{1-x}Fe_xO₃ ($0 \leq x \leq 0.1$) compounds have minutely decreased with increasing Fe- doping concentration (x). K. Asokan *et al.* [10] reported

that Co, Ni and Cu doping at Mn-site in hexagonal YMnO₃ with a specific composition of 1/3 would improve the structural and magnetic properties. L. Jevvrey *et al.* [12] proposed that the magnetic transition temperature T_N of hexagonal YMn_{1-x}Cu_xO₃ had decreased from 70 K down to 49 K when x went from 0 to 0.15. A. M. Zhang *et al.* [13] revealed that the polycrystalline YMn_{1-x}Zn_xO₃ with low Zn doping concentration ($x < 0.1$) maintained single phase which demonstrated hexagonal structure with space group of $P6_3cm$, and the T_N temperatures were respectively 75 K, 65 K and 60 K with $x = 0, 0.04$ and 0.08 .

As mentioned above, a systematic understanding of doping effect on T_N is still lacking although a number of experimental results were given in TM doping YMn_{0.9}TM_{0.1}O₃ (TM = Ti~Zn) bulks. Besides, it remains to be elucidated how the antiferromagnetic interactions and Néel temperatures are modified by dopant incorporation in hexagonal manganite films [14]. In the work, we have firstly used the first-principles method to calculate a variety of TM elements from Ti to Zn atoms doping at the Mn site, and investigate how such doping affects the structural and magnetic properties of hexagonal YMn_{0.917}TM_{0.083}O₃ bulks (approximating to experimental YMn_{0.9}TM_{0.1}O₃ compositions [5, 6, 7, 8, 9, 10, 11, 12, 13]). Then we have also studied the effect of Ti, V, Cr and Fe doping on magnetic properties and discussed the varied electronic structures of TMO₅ in the YMn_{0.917}TM_{0.083}O₃ film configurations, which could provide more understanding towards the designing of new generation multifunctional devices.

2. Calculation

We have performed first-principles density-functional theory (DFT) calculations within the generalized gradient approximation (GGA) [15] using the Vienna *ab initio* Simulation Package (VASP) [16, 17]. The eigenstates of electron wave functions were expanded on a plane-wave basis set using pseudopotentials to describe the electron-ion interactions within the projector augmented-wave approach [18] (PAW). The Monkhorst-Pack (MP) scheme [19] is used for the k -point sampling and the Brillouin zone integration is performed with the Gaussian smearing method. The plane-wave basis energy cutoff is chosen as 500 eV. We respectively treated 11 valence electrons for Y ($4s^2 4p^6 5s^2 4d^1$), 15 for Mn ($3s^2 3p^6 4s^2 3d^5$), and 6 for oxygen ($2s^2 2p^4$). The atomic positions are fully relaxed until atomic forces are less than 10 meV/Å and the total energy is obtained when it converges to 0.1 meV in the electronic self-consistent loop. In the calculations, the Perdew-Burke-Ernzerhof (PBE) [15] form was chosen as the exchange-correlation potentials within the DFT + U scheme. The DFT+U integrals, determined by the PAW on-site occupancies and the on-site electron-electron interaction, are normally specified in terms of the effective on site Coulomb and exchange parameters, U and J [20]. Here, the values of U = 8.0 eV and J = 0.88 eV are applied for the Mn 3d states [21]. U_{eff} is generally

expressed as the difference between two parameters ($U-J$), which determines an orbital-dependent correction to the DFT energy. According to the reported literatures [22, 23, 24, 25, 26, 27, 28, 29], the proper Hubbard correlation item U_{eff} values $U_{\text{eff}}(\text{Ti}) = 3.2$ eV, $U_{\text{eff}}(\text{V}) = 2.64$ eV, $U_{\text{eff}}(\text{Cr}) = 3.0$ eV, $U_{\text{eff}}(\text{Fe}) = 4.0$ eV, $U_{\text{eff}}(\text{Co}) = 6.0$ eV, $U_{\text{eff}}(\text{Ni}) = 4.7$ eV, $U_{\text{eff}}(\text{Cu}) = 7.05$ eV, $U_{\text{eff}}(\text{Zn}) = 8.0$ eV are adopted using the Dudarev implementation [30] in the following calculations. To be close to the doping concentration $x = 0.1$ of stoichiometric component $\text{YMn}_{1-x}\text{TM}_x\text{O}_3$ (TM = Ti ~ Zn) in the experimental reports [5, 6, 7, 8, 9, 10, 11, 12, 13], we built the supercell of a theoretical formula $\text{YMn}_{0.917}\text{TM}_{0.083}\text{O}_3$ bulk with twelve formula units, in which one of 12 Mn atoms was substituted by a TM atom (shown in Fig. 1(a)). For each computational cell of hexagonal $\text{YMn}_{0.917}\text{TM}_{0.083}\text{O}_3$ (TM = Ti ~ Zn) bulks (60 atoms) and the $\text{YMn}_{0.917}\text{TM}_{0.083}\text{O}_3(001)/\text{MgO}(001)$ (TM = Ti, V, Cr and Fe) film [31] configurations (178 atoms) (shown in Fig. 1(b)), we considered three types of magnetic configurations: collinear AFM state, non-collinear magnetic Γ_1 state and ferromagnetic (FM) state. It is found that the magnetic configurations have little effects on the optimized lattice constants. During the geometry optimizations, spin-orbit coupling (SOC) and non-collinear magnetism are regarded to calculate the energies of different magnetic configurations.

3. Results & discussion

3.1. For the hexagonal $\text{YMn}_{0.917}\text{TM}_{0.083}\text{O}_3$ bulks

Firstly we employed the first-principles method to calculate the lattice constants of hexagonal $\text{YMn}_{0.917}\text{TM}_{0.083}\text{O}_3$ (TM = Ti ~ Zn) bulks. Table 1 lists the calculated

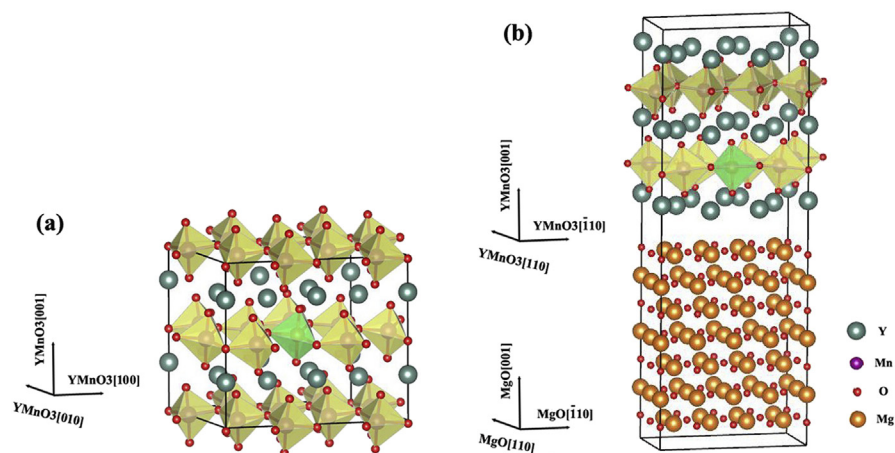


Fig. 1. Schematic of the computational cell considered for (a) the hexagonal $\text{YMn}_{0.917}\text{TM}_{0.083}\text{O}_3$ (TM = Ti ~ Zn) bulk and (b) the $\text{YMn}_{0.917}\text{TM}_{0.083}\text{O}_3(001)/\text{MgO}(001)$ (TM = Ti, V, Cr and Fe) film configurations, where pine green, purple, red and orange spheres indicate Y, Mn, O and Mg atoms, respectively. On the MnO layer, each Mn atom is surrounded by bipyramidal oxygen atoms which form a MnO_5 trigonal bipyramid (light yellow). The Mn atom in the green bipyramid will be substituted by a TM atom in the work.

Table 1. Calculated lattice constants and Néel temperatures for the $\text{YMn}_{0.917}\text{TM}_{0.083}\text{O}_3$ compositions compared to experimental values of hexagonal $\text{YMn}_{0.9}\text{TM}_{0.1}\text{O}_3$ (TM = Ti~Zn) bulks.

TM	Experimental data			Calculated values		
	(<i>a</i> , <i>c</i>) (Å)	Volume (Å ³)	<i>T_N</i> (K)	(<i>a</i> , <i>c</i>) (Å)	Volume (Å ³)	<i>T_N</i> (K)
Ti	6.141, 11.370	371.35 [6]	55 [6]	6.175, 11.535	380.89	47
V				6.131, 11.433	372.16	63
Cr	6.143, 11.415	373.04 [34]	89 [7], 86 [8]	6.202, 11.539	384.37	99
Mn	6.120, 11.400	369.93 [35]	73 [7], 75 [35]	6.121, 11.408	370.14	70
Fe	6.136, 11.429	372.64 [6]	60 [6], 67 [9]	6.163, 11.460	376.95	62
Co				6.170, 11.492	378.86	63
Ni	42 [11]			6.227, 11.310	379.78	62
Cu	6.152, 11.382	373.05 [11]	59 [12]	6.198, 11.562	384.63	64
Zn	6.179, 11.410	377.25 [12]	70 [5], 60 [13]	6.225, 11.458	384.50	67

lattice constants for the $\text{YMn}_{0.917}\text{TM}_{0.083}\text{O}_3$ compared to the earlier experimental values of bulk hexagonal $\text{YMn}_{0.9}\text{TM}_{0.1}\text{O}_3$ (TM = Ti~Zn). It can be seen that the lattice parameter differences between the calculated and experimental data are less than 1.0%, although the calculated compositions $\text{YMn}_{0.917}\text{TM}_{0.083}\text{O}_3$ are slightly different from the experimental constituents $\text{YMn}_{0.9}\text{TM}_{0.1}\text{O}_3$. The calculated results are in good agreement with the experiments, which proves the reliability of our computations for the doping $\text{YMn}_{0.917}\text{TM}_{0.083}\text{O}_3$ systems (including the hexagonal $\text{YMn}_{0.917}\text{TM}_{0.083}\text{O}_3$ (TM = Ti ~ Zn) bulks and the $\text{YMn}_{0.917}\text{TM}_{0.083}\text{O}_3(001)/\text{MgO}(001)$ (TM = Ti, V, Cr and Fe) film configurations).

To study the doping effects on the magnetic properties of hexagonal $\text{YMn}_{0.917}\text{TM}_{0.083}\text{O}_3$ (TM = Ti~Zn) bulks, the theoretical magnetic transition temperatures (T_N) have been calculated based on the different magnetic structures (such as collinear AFM state, non-collinear magnetic Γ_1 state and FM state) and the nearest-neighbor spin-exchange interactions [36]. In all doping systems, the lowest energy state is the Γ_1 state, whose lattice parameters are listed in Table 1. The calculated Néel temperatures are also listed. The formula to calculate Néel temperatures will be shown in Section 3.2. Fig. 2 shows that the calculated Néel temperatures varied with doping elements (TM) in the $\text{YMn}_{0.917}\text{TM}_{0.083}\text{O}_3$ bulks, and compared with the reported experimental values of $\text{YMn}_{0.9}\text{TM}_{0.1}\text{O}_3$ (TM = Ti ~ Zn). It can be seen that the calculated T_N results clearly depend on doping elements, which agree well with those obtained from experiments. These confirm the sensitivity of magnetic properties to slight perturbations for the hexagonal YMnO_3 systems. And it is noteworthy that the Cr doping would induce a Néel temperature (T_N) increase higher than the others TM substitutions in the $\text{YMn}_{0.917}\text{TM}_{0.083}\text{O}_3$ bulks.

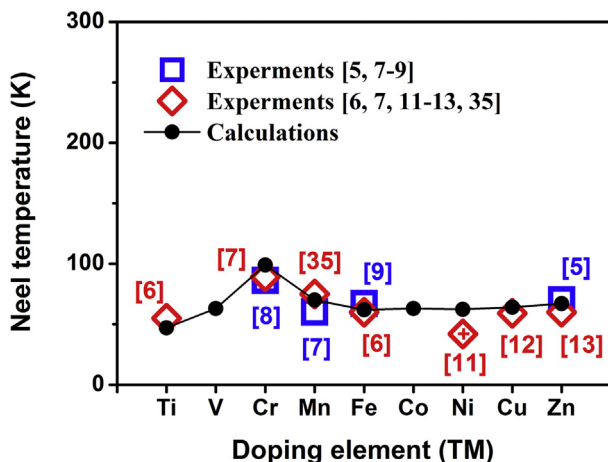


Fig. 2. Variation of Néel temperatures with the TM dopant in $\text{YMn}_{0.917}\text{TM}_{0.083}\text{O}_3$ (TM = Ti ~ Zn) bulks in comparison with the experimental data. In the figure, the symbol \diamond denotes the reference value from the experimental phase of $\text{YMn}_{0.8}\text{Ni}_{0.2}\text{O}_3$ [11].

As is well known, the structural parameters can be varied by suitable substitution and hence one can tune the magnetic property in these types of materials [39]. In the $\text{YMn}_{0.917}\text{TM}_{0.083}\text{O}_3$ compounds, doping at Mn-site would cause the structural distortion of TMO_5 bipyramid, the magnetic ordering could be driven by the spin-exchange interaction, and the magnetic interaction strength might depend on the bond length and bond angle. Fig. 3 shows that bond length sums $\{(\text{TM}-\text{O}1) + (\text{TM}-\text{O}2)$, and $(\text{TM}-\text{O}3) + (\text{TM}-\text{O}4)\}$ and bond length ratios $\{(\text{TM}-\text{O}1)/(\text{TM}-\text{O}2)$, and $(\text{TM}-\text{O}3)/(\text{TM}-\text{O}4)\}$ change with doping elements (TM) for TMO_5 bipyramids in the hexagonal $\text{YMn}_{0.917}\text{TM}_{0.083}\text{O}_3$ bulks. The inset of Fig. 3 displays the TMO_5 bipyramid structure in which the TM atom is located at the center. It is noted in Fig. 3 that the apical bond length sum $\{(\text{TM}-\text{O}1) + (\text{TM}-\text{O}2)\}$ are always smaller than the planar bond length sum $\{(\text{TM}-\text{O}3) + (\text{TM}-\text{O}4)\}$, which indicates that TM doping

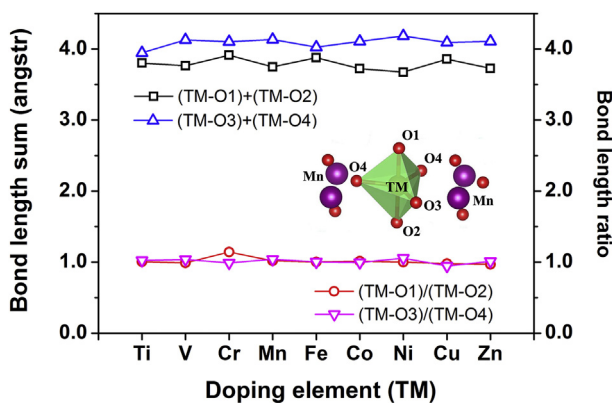


Fig. 3. Bond length sums and bond length ratios for TMO_5 bipyramids in hexagonal $\text{YMn}_{0.917}\text{TM}_{0.083}\text{O}_3$ bulks dependence on doping elements (TM) from Ti to Zn. The inset is the structural representation of TMO_5 bipyramid.

would not change the basic structural characteristics of TMO_5 bipyramids. It is also noted in Fig. 3 that the bond length ratios $\{(\text{TM-O1})/(\text{TM-O2}), \text{ and } (\text{TM-O3})/(\text{TM-O4})\}$ are almost same (around the value of 1.0). However, the ratio value of (TM-O1) to (TM-O2) has a notable deviation when Cr is the doping element. This might be one reason why the Néel temperature of $\text{YMn}_{0.917}\text{Cr}_{0.083}\text{O}_3$ exhibits an increase higher than the others $\text{YMn}_{0.917}\text{TM}_{0.083}\text{O}_3$ bulks in Fig. 2.

To further investigate the structural variations of TMO_5 bipyramids (shown in the inset of Fig. 3), Figs. 4 and 5 respectively demonstrate the bond lengths and bond angles dependence on doping elements (TM) from Ti to Zn. Table 2 lists the calculated main bond lengths and bond angles for TMO_5 bipyramid in $\text{YMn}_{0.917}\text{TM}_{0.083}\text{O}_3$ bulks, compared to available experimental values in $\text{YMn}_{0.9}\text{TM}_{0.1}\text{O}_3$ (TM = Ti, Mn and Fe) from the previous report [6], which have once again proven that our calculated results are in good agreement with the experimental ones. In Figs. 4 and 5, main bond lengths and bond angles (two structural features) of TMO_5 bipyramids are respectively changed with different doping elements. It is noteworthy that the variations of TM-O1 distances show a sudden rise when the bond length is Cr-O1 (in Fig. 4), meanwhile the fluctuating curves of O4-TM-O4 angles exhibit a biggest drop at O4-Cr-O4 angle (in Fig. 5), both of which suggest a significant structural distortion occurred in the CrO_5 bipyramid. When compared between the CrO_5 and the MnO_5 bipyramid structures, it is clear in Fig. 3 that the planar bond length sum $\{(\text{Cr-O3}) + (\text{Cr-O4})\}$ is less than the $\{(\text{Mn-O3}) + (\text{Mn-O4})\}$ distance, but the apical bond length sum $\{(\text{Cr-O1}) + (\text{Cr-O2})\}$ is larger than the $\{(\text{Mn-O1}) + (\text{Mn-O2})\}$ distance. As results, the lengthening Cr-O1 distance would decrease the exchange interactions along the [001] direction, and the reduced O4-Cr-O4 angle would cause the bonding strength increase on the Cr-O plane. That is to say, the significant changes of two structural features of CrO_5

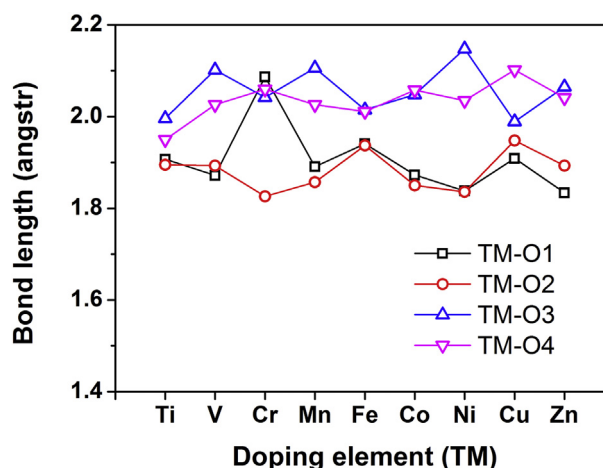


Fig. 4. Main bond lengths for TMO_5 bipyramids in hexagonal $\text{YMn}_{0.917}\text{TM}_{0.083}\text{O}_3$ bulks dependence on doping elements (TM) from Ti to Zn.

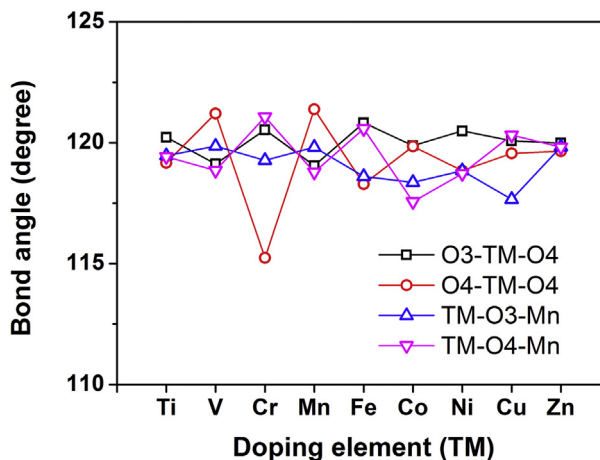


Fig. 5. Main bond angles for TMO₅ bipyramids in hexagonal YMn_{0.917}TM_{0.083}O₃ bulks dependence on doping elements (TM) from Ti to Zn.

Table 2. Calculated main bond lengths and bond angles for TMO₅ bipyramid in YMn_{0.917}TM_{0.083}O₃ compared to available experimental values [6] in YMn_{0.9}TM_{0.1}O₃ (TM = Ti, Mn and Fe).

Geometrical parameter	Ti	Ti	Mn	Mn	Fe	Fe
	Exp.	Cal.	Exp.	Cal.	Exp.	Cal.
TM-O1 (Å)	1.940	1.907	1.900	1.891	1.880	1.941
TM-O2 (Å)	1.790	1.895	1.860	1.857	1.820	1.937
TM-O3 (Å)	2.120	1.966	2.082	2.106	2.080	2.015
TM-O4 (Å)	2.023	1.950	2.039	2.026	2.043	2.011
TM-O3-Mn(°)	119.40	119.46	119.24	119.82	119.00	118.61
TM-O4-Mn(°)	119.20	119.42	118.51	118.77	119.10	120.57

bipyramid would increase the exchange interactions of planar Cr-O bonds and result in a more stable magnetic state, and eventually change the structural and magnetic properties in the hexagonal YMn_{0.917}Cr_{0.083}O₃ bulk system (inducing the highest T_N peak as shown in Fig. 2).

3.2. For the YMn_{0.917}TM_{0.083}O₃(001)/MgO(001) film configurations

By performing DFT calculations, we have also examined variations of electronic structures and magnetic properties of hexagonal YMn_{0.917}TM_{0.083}O₃(001)/MgO(001) (TM = Ti, V, Cr and Fe) film configurations. Based on the different Néel spin states (collinear AFM state, non-collinear magnetic Γ_1 state and FM state) and the nearest-neighbor spin-exchange interactions, the theoretical magnetic parameters such as transition temperatures (T_N) and Curie-Weiss temperatures

(Θ_{CW}) have been calculated [36, 37, 38] to study the doping effects of Ti, V, Cr and Fe atom at Mn site on magnetic properties of $\text{YMn}_{0.917}\text{TM}_{0.083}\text{O}_3(001)/\text{MgO}(001)$ configurations. The nearest-neighbor spin-exchange coupling J_{nn} in the hexagonal structure of YMnO_3 can be calculated as: [36]

$$J_{nn} = \frac{1}{36(\sqrt{3} + 2)}(E_{\Gamma_1} - E_{AFM}) + \frac{1}{216}(E_{AFM} - E_{FM})$$

where E_{AFM} , E_{Γ_1} and E_{FM} are respectively total energies for different magnetic configurations (three Néel spin states) as collinear AFM state, non-collinear magnetic Γ_1 state and FM state. Then according to L. Capriotti *et al.* [37, 38], the magnetic transition temperature can be estimated as $T_N = -0.3J_{nn}\left(S + \frac{1}{2}\right)^2$ using the nearest-neighbor spin-exchange coupling J_{nn} and the absolute value of Mn spin S . The theoretical Curie-Weiss temperature can be calculated using the expression: $\Theta_{CW} = \left(\frac{1}{3}\right) \cdot Z \cdot J_{nn} \cdot S \cdot (S + 1)$ [36], where Z is the number of nearest neighbors.

Table 3 lists the calculated values of magnetic parameters of $\text{YMn}_{0.917}\text{TM}_{0.083}\text{O}_3(001)/\text{MgO}(001)$ (TM = Ti, V, Cr and Fe) configurations. It can be found that Cr doping would also induce a T_N increase of film configuration similar to the $\text{YMn}_{0.917}\text{Cr}_{0.083}\text{O}_3$ bulk, however, others doping (Ti, V and Fe) would make Néel temperatures reduced to some degree. As we know, the antiferromagnetic ordering temperature of YMnO_3 is much lower than the absolute value of the Curie-Weiss temperature. Due to the antiferromagnetic interactions, the Curie-Weiss temperatures are negative in the film configurations. It is noted that the variation trends of absolute value of Curie-Weiss temperature $|\Theta_{CW}|$ are consistent with the Néel temperatures. With the doping elements (Ti, V, Cr and Fe), the calculated effective magnetic moments (μ_{eff}) have decreased slightly when compared to pure $\text{YMnO}_3(001)/$

Table 3. Calculated values of magnetic parameters of $\text{YMn}_{0.917}\text{TM}_{0.083}\text{O}_3(001)/\text{MgO}(001)$ (TM = Ti, V, Cr and Fe) configurations. ΔT_N is a difference between the Néel temperature of a doped compound and the pure one. The effective magnetic moment is averaged magnetic moment of TM and Mn in the doped system.

TM	T_N (K)	ΔT_N (K)	Θ_{CW} (K)	μ_{eff} (μ_B)	f
Ti	123	-24	-789	4.50	6.415
V	121	-26	-778	4.53	6.429
Cr	161	14	-1031	4.62	6.404
Mn	147 [31]	0	-946	4.70	6.435
Fe	118	-29	-757	4.61	6.415

MgO(001) configuration. Nevertheless, the μ_{eff} values of Cr, Mn and Fe doping are comparable within the difference (2%). The value of parameter $f = \frac{|\Theta_{CW}|}{T_N}$ is a magnetic frustration factor which can be used as a measure of the spin frustration strength. If the ratio f is larger than 10, the spin system should be classified as the one with strong geometrical frustration since the value cannot be explained by the simple mean-field theory [40]. For the hexagonal YMnO₃ bulk, the calculated Θ_{CW} is -468 K and T_N is 73 K, then the frustration factor ($f = 6.41$) can be obtained; which is very close to the experimental value ($f = 6.43$) [9]. For the YMn_{0.917}TM_{0.083}O₃(001)/MgO(001) configurations, it can be seen in Table 3 that the f parameters remain almost the same (the deviations are less than 0.5%) and seem to be independent on the doping elements (TM = Ti, V, Cr and Fe). Because the magnetic interaction strength depends on the extent of orbital overlap and the covalent bond, we next calculated the orbital-resolved density of states (DOS) for further understanding of TM doping effect on electronic structure characteristics of TMO₅ bipyramids in YMn_{0.917}TM_{0.083}O₃(001)/MgO(001) configurations.

As we know, the crystal field of hexagonal YMnO₃ splits the Mn d orbitals into two doublets (e_{1g} and e_{2g}) and a singlet (a_{1g}). In the TMO₅ bipyramids (shown in the inset of Fig. 3), the d_z^2 orbitals (a_{1g}) would like to point towards the apical oxygens (O1 and O2) favorable to the bonding {(TM-O1)+(TM-O2)}, and the d_{xy} and $d_{x^2-y^2}$ orbitals (e_{2g}) towards the planar oxygens (O3 and O4) in favor of covalent bonding {(TM-O3)+(TM-O4)}. Fig. 6 shows the orbital-resolved DOSs of the individual TM (TM = Ti, V, Cr, Mn and Fe) d for TMO₅ bipyramids in YMn_{0.917}TM_{0.083}O₃(001)/MgO(001) configurations (d_{yz} and d_{zx} not shown). In the energy range between -7.6 eV and -3.1 eV where O p orbitals locate, the TM orbital d_z^2 DOS's will be responsible for the d_z^2 (TM)– p_z (O1 or O2) interaction, and the TM d_{xy} (shaded gray in Fig. 6) and $d_{x^2-y^2}$ orbitals will be in charge of

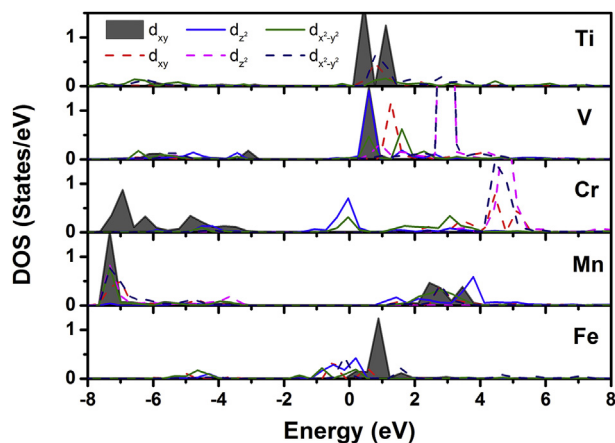


Fig. 6. Orbital-resolved density of states of the individual TM (TM = Ti, V, Cr, Mn and Fe) d for TMO₅ bipyramids in YMn_{0.917}TM_{0.083}O₃(001)/MgO(001) configurations as a function of energy ($E-E_F$), in which E_F is the Fermi energy. Solid and dashed lines denote majority and minority states, respectively.

hybridization with the in-plane O3(O4) p_x and p_y . Note that the occupied states of Cr e_{2g} (d_{xy} and $d_{x^2-y^2}$) orbitals illustrate a stronger hybridization trend with O3(O4) (p_x and p_y) orbitals than the other TM (Ti, V, Mn and Fe) doping's DOS states, and the occupied states of Cr a_{1g} (d_z^2) orbitals exhibit a less interaction with O1(O2) (p_z) orbitals than the states of V and Mn orbitals (energy ranging from -7.6 eV to -3.1 eV), all of which suggest that the increase of orbital interactions involved in the planar Cr-O covalent bonds, and the slight decrease of apical Cr-O orbital interactions have both accounted for the increase of magnetic ordering temperature in the $\text{YMn}_{0.917}\text{Cr}_{0.083}\text{O}_3(001)/\text{MgO}(001)$ configuration.

4. Conclusions

In conclusion, the Mn-site doping behaviors of hexagonal $\text{YMn}_{0.917}\text{TM}_{0.083}\text{O}_3$ systems have been systematically studied by using the first-principles method. The calculated Néel temperatures, varied with doping elements in $\text{YMn}_{0.917}\text{TM}_{0.083}\text{O}_3$ bulks, are in agreement with the reported experimental values of $\text{YMn}_{0.9}\text{TM}_{0.1}\text{O}_3$ (TM = Ti ~ Zn). We have found that the structural changes of TMO_5 bipyramids would lead to the transformations of magnetic properties. The planar TM-O bonds and O-TM-O angles of TMO_5 bipyramid are both important structural features for the changes of magnetic ordering temperatures. Then the doping effects of transition metal Ti, V, Cr and Fe at Mn site have also been predicted on the varied magnetic properties of $\text{YMn}_{0.917}\text{TM}_{0.083}\text{O}_3(001)/\text{MgO}(001)$ film configurations, in which the Cr doping would also induce a T_N increase higher than the others doping similar to the $\text{YMn}_{0.917}\text{Cr}_{0.083}\text{O}_3$ bulk. By analyses of electronic structures, it can be found that the occupied states of TM e_{2g} (d_{xy} and $d_{x^2-y^2}$) and TM a_{1g} (d_z^2) orbitals are simultaneously responsible for the strength of covalent bonds and eventually influence on the magnetic transition temperatures. These insightful results could provide more understanding towards the transition metal doping effect on the structural, electronic and magnetic properties of YMnO_3 films and the designing of new generation multifunctional devices.

Declarations

Author contribution statement

Dong Chen: Analyzed and interpreted the data, Wrote the paper.

Yu-Jia Wang: Conceived and designed the analysis.

Yin-Lian Zhu, Xiu-Liang Ma: Contributed analysis tools or data.

Funding statement

This work was supported by the National Natural Science Foundation of China (NSFC) (51371176, 51571197 and 51671194), and the Frontier Science Key

Programs of the Chinese Academy of Sciences (QYZDJ-SSW-JSC010). Dong Chen was supported by the Special Program for Applied Research on Super Computation of the NSFC-Guangdong Joint Fund (the second phase) under Grant No. U1501501.

Competing interest statement

The authors declare no conflict of interest.

Additional information

No additional information is available for this paper.

Acknowledgements

We thank Dr. T. Sasaki and Dr. I Solovyev (Computational Materials Science Unit, National Institute for Materials Science, 1-1 Namiki, Tsukuba, Japan) for good suggestions and fruitful discussions.

References

- [1] B.B. Van Aken, T.T.M. Palstra, A. Filippetti, N.A. Spaldin, The origin of ferroelectricity in magnetoelectric YMnO_3 , *Nat. Mater.* 3 (2004) 164–170.
- [2] A. Muñoz, J.A. Alonso, M.J. Martínez-Lope, M.T. Casáis, J.L. Martínez, M.T. Fernández-Daíz, Magnetic structure of hexagonal RMnO_3 ($\text{R}=\text{Y}, \text{Sc}$): thermal evolution from neutron powder diffraction data, *Phys. Rev. B* 62 (2000) 9498–9510.
- [3] T. Katsufuji, S. Mori, M. Masaki, Y. Moritomo, N. Yamamoto, H. Takagi, Dielectric and magnetic anomalies and spin frustration in hexagonal RMnO_3 ($\text{R}=\text{Y}, \text{Yb}, \text{and Lu}$), *Phys. Rev. B* 64 (2001) 104419.
- [4] A.J. Overton, J.L. Best, I. Saratovsky, M.A. Hayward, Influence of topotactic reduction on the structure and magnetism of the multiferroic YMnO_3 , *Chem. Mater.* 21 (2009) 4940–4948.
- [5] J. Park, M. Kang, J. Kim, S. Lee, K.H. Jang, A. Pirogov, J.G. Park, C. Lee, S.H. Park, H.C. Kim, Doping effects of multiferroic manganites $\text{YMn}_{0.9}\text{X}_{0.1}\text{O}_3$ ($\text{X}=\text{Al}, \text{Ru}, \text{and Zn}$), *Phys. Rev. B* 79 (2009) 064417.
- [6] N. Sharma, A. Das, C.L. Prajapat, S.S. Meena, Spin reorientation behavior in $\text{YMn}_{1-x}\text{M}_x\text{O}_3$ ($\text{M}=\text{Ti}, \text{Fe}, \text{Ga}; x=0,0.1$), *J. Magn. Magn. Mater.* 348 (2013) 120–127.
- [7] T.C. Han, I.C. Wu, H.K. Hsu, Effects of Cr doping on the magnetic properties of multiferroic YMnO_3 , *J. Appl. Phys.* 115 (2014) 17D906.

- [8] F. Wan, X.J. Bai, K.K. Song, X. Lin, X.M. Han, J.B. Zheng, C.D. Cao, Structure and magnetism of Cr-doped h-YMnO₃, *J. Magn. Magn. Mater.* 424 (2017) 371–375.
- [9] S. Namdeo, A.K. Sinha, M.N. Singh, A.M. Awasthi, Investigation of charge states and multiferroicity in Fe-doped h-YMnO₃, *J. Appl. Phys.* 113 (2013) 104101.
- [10] K. Asokan, Y.S. Chen, C.W. Pao, H.M. Tsai, C.W.O. Lee, C.H. Lin, H.C. Hsueh, D.C. Ling, W.F. Pong, J.W. Chiou, M.H. Tsai, O. Peña, C. Moure, Effect of Co, Ni, and Cu substitution on the electronic structure of hexagonal YMnO₃ studied by x-ray absorption spectroscopy, *Appl. Phys. Lett.* 95 (2009) 131901.
- [11] O. Peña, M. Bahout, D. Gutiérrez, J.F. Fernández, P. Durán, C. Moure, Critical behavior in the perovskite-like system Y(Ni,Mn)O₃, *J. Phys. Chem. Solid.* 61 (2000) 2019–2024.
- [12] L. Jouvrey, O. Peña, A. Moure, C. Moure, Synthesis and magnetic properties of hexagonal Y(Mn,Cu)O₃ multiferroic materials, *J. Magn. Magn. Mater.* 324 (2012) 717–722.
- [13] A.M. Zhang, G.T. Zhou, L. Zheng, X.S. Wu, Magnetic properties and local microstructures in Zn-doped YMnO₃, *J. Appl. Phys.* 115 (2014) 133907.
- [14] J. Fontcuberta, Multiferroic RMnO₃ thin films, *C. R. Physique* 16 (2015) 204–226.
- [15] J.P. Perdew, K. Burke, M. Ernzerhof, Generalized gradient approximation made simple, *Phys. Rev. Lett.* 77 (1996) 3865–3868.
- [16] G. Kresse, J. Furthmüller, Efficient iterative schemes for ab initio total-energy calculations using a plane-wave basis set, *Phys. Rev. B* 54 (1996) 11169–11186.
- [17] G. Kresse, D. Joubert, From ultrasoft pseudopotentials to the projector augmented-wave method, *Phys. Rev. B* 59 (1999) 1758–1775.
- [18] P.E. Blöchl, Projected augmented-wave method, *Phys. Rev. B* 50 (1994) 17953–17979.
- [19] H.J. Monkhorst, J.D. Pack, Special points for Brillouin-zone integrations, *Phys. Rev. B* 13 (1976) 5188–5192.
- [20] Available online at <http://cms.mpi.univie.ac.at/vasp/guide/vasp.html>.
- [21] I.S. Elfimov, V.I. Anisimov, G.A. Sawatzky, Orbital Ordering, Jahn-Teller distortion, and anomalous X-Ray scattering in Manganates, *Phys. Rev. Lett.* 82 (1999) 4264–4267.

- [22] X. Huang, Y. Tang, S. Dong, Strain-engineered A type antiferromagnetic order in YTiO_3 : a first principles calculation, *J. Appl. Phys.* 113 (2013) 17E108.
- [23] I.V. Solovyev, Lattice distortion and magnetism of $3d-t_{2g}$ perovskite oxides, *Phys. Rev. B* 74 (2006) 054412.
- [24] N. Ray, U.V. Waghmare, Coupling between magnetic ordering and structural instabilities in perovskite biferroics: a first-principles study, *Phys. Rev. B* 77 (2008) 134112.
- [25] J. Alaria, P. Borisov, M.S. Dyer, T.D. Manning, S. Lepadatu, M.G. Cain, E.D. Mishina, N.E. Sherstyuk, N.A. Ilyin, J. Hadermann, D. Lederman, J.B. Claridge, M.J. Rosseinsky, Engineered spatial inversion symmetry breaking in an oxide heterostructure built from isosymmetric room-temperature magnetically ordered components, *Chem. Sci.* 5 (2014) 1599–1610.
- [26] Z. Zhu, J. Guo, Y. Jia, X. Hu, Electronic structure and evolution of spin state in YCoO_3 , *Phys. B* 405 (2010) 359.
- [27] M. Szwajca, F. Calvayrac, Modelling noncollinear spin structure in YNiO_3 perovskite: a GGA+U APW approach, *J. Phys. Conf.* 289 (2011) 012002.
- [28] P. Blaha, K. Schwarz, P. Novák, Electric field gradients in cuprates: does LDA+U give the correct charge distribution? *Int. J. Quant. Chem.* 101 (2005) 550–556.
- [29] A. Boonchun, W.R.L. Lambrecht, Electronic structure of defects and doping in ZnO : oxygen vacancy and nitrogen doping, *Phys. Status Solidi B* 250 (2013) 2091–2101.
- [30] S.L. Dudarev, G.A. Botton, S.Y. Savrasov, C.J. Humphreys, A.P. Sutton, Electron-energy-loss spectra and the structural stability of nickel oxide: An LSDA+U study, *Phys. Rev. B* 57 (1998) 1505–1509.
- [31] We have investigated the electronic structures and the magnetic state transitions of hexagonal YMnO_3 films under different strain states according to the experimental observations [32, 33], and elucidated that the magnetic transition temperature would be increased when the in-plane strain is tensile in the $\text{YMnO}_3(001)/\text{MgO}(001)$ film. The details will be discussed in a Forthcoming Publication.
- [32] K.H. Wu, H.J. Chen, Y.T. Chen, C.C. Hsieh, C.W. Luo, T.M. Uen, J.Y. Juang, J.Y. Lin, T. Kobayashi, M. Gospodinov, Marked enhancement of Néel temperature in strained YMnO_3 thin films probed by femtosecond spectroscopy, *EPL* 94 (2011) 27006.

- [33] K.H. Wu, H.J. Chen, C.C. Hsieh, C.W. Luo, T.M. Uen, J.Y. Lin, J.Y. Juang, Epitaxial-strain effects on electronic structure and magnetic properties of hexagonal YMnO₃ thin films studied by femtosecond spectroscopy, *J. Supercond. Nov. Magn.* 26 (2013) 801–807.
- [34] F. Wan, X. Lin, X. J Bai, X.M. Han, K.K. Song, J.B. Zheng, C.D. Cao, Crystalline structure and dielectric properties of multiferroic Cr-doped YMnO₃, *J. Mater. Sci. Mater. Electron.* 27 (2016) 3082–3087.
- [35] S. Lee, A. Pirogov, M. Kang, K.H. Jang, M. Yonemura, T. Kamiyama, S.W. Cheong, F. Gozzo, N. Shin, H. Kimura, Y. Noda, J.G. Park, Giant magneto-elastic coupling in multiferroic hexagonal manganites, *Nature* 451 (2008) 805–808.
- [36] C.G. Zhong, X.F. Jiang, H.L. Yu, Q. Jiang, J.H. Fang, Z.Y. Li, First-principles studies of the magnetic structure and exchange interactions in the frustrated multiferroic YMnO₃, *J. Magn. Magn. Mater.* 321 (2009) 1260–1265.
- [37] L. Capriotti, R. Vaia, A. Cuccoli, V. Tognetti, Phase transitions induced by easy-plane anisotropy in the classical Heisenberg antiferromagnet on a triangular lattice: a Monte Carlo simulation, *Phys. Rev. B* 58 (1998) 273–281.
- [38] L. Capriotti, A. Cuccoli, V. Tognetti, P. Verrucchi, R. Vaia, Thermodynamics of the quantum easy-plane antiferromagnet on the triangular lattice, *Phys. Rev. B* 60 (1999) 7299–7303.
- [39] S.L. Samal, T. Magdaleno, K.V. Ramanujachary, S.E. Lofland, A.K. Ganguli, Enhancement of magnetic ordering temperature in iron substituted ytterbium manganate (YbMn_{1-x}Fe_xO₃), *J. Solid State Chem.* 183 (2010) 643–648.
- [40] B. Paul, S. Chatterjee, A. Roy, A. Midya, P. Mandal, V. Grover, A.K. Tyagi, Geometrically frustrated GdInO₃: an exotic system to study negative thermal expansion and spin-lattice coupling, *Phys. Rev. B* 95 (2017) 054103.